JPE 16-4-27

http://dx.doi.org/10.6113/JPE.2016.16.4.1526
ISSN(Print): 1598-2092 / ISSN(Online): 2093-4718

Improved Decoupled Control and Islanding Detection of Inverter-Based Distribution in Multibus Microgrid Systems

Smitha Joyce Pinto† and Gayadhar Panda*

†,*Department of Electrical Engineering, National Institute of Technology Meghalaya, Shillong, India

Abstract

This work mainly discusses an accurate and fast islanding detection based on fractional wavelet packet transform (FRWPT)for multibus microgrid systems. The proposed protection scheme uses combined desirable features retrieved from discrete fractional Fourier transform (FRFT) and wavelet packet transform (WPT) techniques, which provides precise time–frequency information on minute perturbation signals introduced in the system. Moreover, this study focuses on the design of decoupling control with a distributed controller based on state feedback for the efficient operation of microgrid systems that are transitioning from the grid-connected mode to the islanded mode. An IEEE 9-bus test system with inverter based distributed generation (DG) units is considered for islanding assessment and smooth operation. Finally, tracking errors are greatly reduced with stability improvement based on the proposed controller. FRWPT based islanding detection is demonstrated via a time domain simulation of the system. Simulated results show an improvement in system stability with the application of the proposed controller and accurate islanding detection based on the FRWPT technique in comparison with the results obtained by applying the wavelet transform (WT) and WPT.

Keywords: Decoupled controller, Fractional wavelet packet transform, Islanding detection, Microgrid, Observer, Power flow control

I. INTRODUCTION

The growing demand for electricity has widened the use of distributed generation (DG) systems in modern power grids. The best method for integrating renewable energy into power grids is the microgrid formation technique, which involves grouping a few DG units and controllable loads. The integration of DG units facilitates the reduction of line losses and eliminates the need for dependence on fossil fuel for electricity generation and improved system reliability. The extensive application of DGs raises few challenges, such as power quality monitoring, efficient operation, and system safety, which are generally analyzed under various transient and steady state conditions. Therefore, a suitable decentralized control technique for the efficient operation of microgrids under grid-connected and islanded modes is highly necessary [1]-[3]. Over the past few years, many control strategies have been applied to the operation of inverter based DG systems with LCL filters, and their performance is well documented in the literature [4]-[6]. The combined state-space design for the placement of observer poles is a powerful control technique in time domain analyses. Adding an observer to system usually improves system stability [7]-[9]. The present study employs an observer based decoupled controller for the efficient operation of microgrid sunder grid-connected and islanded modes. The proposed decoupled control technique can ensure high system stability by tuning the parameters independently.

Rapid and accurate islanding detection is a major challenge that deserves to be addressed to maintain power quality, power restoration, system reliability, and cost. Islanding occurs when DG units and local loads are separated from the main utility grid, which continues to feed power to the local loads. This situation can lead to safety hazards for personnel

Manuscript receive Nov. 12, 2015; accepted Feb. 24, 2016
Recommended for publication by Associate Editor Jae-Do Park.
†Corresponding Author: smitha_joyce@yahoo.co.in
Tel: +91-8212566679, National Institute of Technology Meghalaya
*Department of Electrical Engineering, National Institute of Technology Meghalaya, India

and increased risk of damage to power systems. Therefore, this state of disturbance requires proper identification and protection [10]. The power industries must employ an accurate and fast detection technique for the immediate isolation of DG units at the time of utility fault occurrence/micro-grid isolation. In general, islanding detection techniques are categorized into passive, active, and hybrid methods [11].

In islanding detection, passive protection methods use measured system parameters, such as voltage, current, frequency, and harmonic distortion at DG locations or points of common coupling (PCC). The measured system parameters are compared with pre-defined threshold values for islanding detection. The main drawback of passive islanding detection techniques is the formation of large non detection zones (NDZs), at which these techniques fail to detect islanding. In case of a close mismatch between power generation and load demand, such techniques also fail to identify islanding. Furthermore, caution must be observed when defining threshold values for islanding detection. Otherwise, undesirable tripping signals may emerge and be forwarded to the circuit breaker (CB).Several active detection methods are presented in the literature [12], [13] to overcome the limitations of passive islanding detection schemes.

Active detection schemes are employed by creating controlled external perturbations in the network and monitoring changes in the detection threshold value to detect islanding situation. However, these methods cause the deterioration of the power quality of the system because of injected disturbance signals. Moreover, perturbations are formed in the system at predefined regular time intervals even though such formation is not required under normal operations. If islanding arises immediately after the injection of predefined perturbations, then the system must wait for the next perturbation to determine the electrical grid status [14]. In such a case, the detection of islanding and other power quality disturbances is delayed.

Hybrid methods have been introduced to overcome the aforementioned shortcomings of passive and active detection techniques [15]. These hybrid methods exhibit small NDZs and maintain power quality. However, these methods suffer from high detection time and entail high costs. In this regard, signal processing techniques are mostly used to achieve rapid and accurate islanding detection. Well documented signal processing methods for islanding detection include the Fourier transform (FT), short time Fourier transform (STFT), and WT [16], [17]. WT exhibits excellent time–frequency localization capability and is thus regarded as an effective tool for analyzing power quality disturbances. However, WT based detection schemes suffer from a number of shortcomings, such as batch processing step and detection failure under noisy conditions [18]. In the advancement of WT, other hybrid techniques, such as the neuro-wavelet, robust wavelet and artificial neural network techniques, have been developed [19], [20]. The application of these hybrid techniques delays the detection time [21]-[23]. To achieve a rapid and accurate detection of electrical grid status, we propose a hybrid FRWPT based anti islanding scheme in this study.

II. System Configuration

A typical IEEE 9-bus microgrid system that includes inverter based DG units and various loads is adopted in this study to detect islanding and power quality disturbances as shown in Fig. 1. Under normal operations, the adopted test system comprising various loads and inverter based DG units is connected to the utility grid at the PCC. This system consists of two photovoltaic generation units denoted as DG1 and DG2. The DG units work either in parallel to the utility grid or in isolated mode to feed power to sensitive loads connected in the low distribution feeders when the main CB is open. The schematic diagram of the building blocks for power generation by one DG unit is shown in Fig. 1. The overall microgrid system is controlled by employing an observer based decentralized controller, i.e., each DG unit is locally controlled, as depicted in Fig. 2. However, the information from other non-local feeders is collected using phase measurement units. The overall system parameters are described as follows and are presented in Tables I and II. Table I describes the line parameters, whereas Table II presents the bus data information. These values are used for system simulation study.

1) *Utility Grid*: rated short circuit MVA=2,500, frequency=60 Hz, and base voltage = 120 kV.
2) *Distributed Generations (DGs)*: rating of DG1 and DG2= 80 kW.
3) *Transformers (T, T1, and T2)*:
   For transformer T: power = 47 MW, frequency = 60 Hz, rated voltage = 230 kV/25 kV, base voltage = 25 kV, R_l = 0.0026 p.u., X_l = 0.08 p.u., R_m = 500 p.u., and X_m = 500 p.u.
   For transformers T1 and T2: power =100 kW, frequency= 60 Hz, rated voltage = 425 V/25 kV, base voltage = 25 kV, R_l = 0.001 p.u., X_l = 0.03 p.u., R_m = 500 p.u., and X_m = 500 p.u.
4) *Normal load data*:
   Load A (RL load) = 90 kW, 3 kVAR
   Load B (RL load) = 120 kW, 5 kVAR
   Load C (RL load) = 10 kW, 3 kVAR

III. Decoupled Controller Design

This section describes the design of an improved decoupled controller for each DG unit to allow the operation of a microgrid under grid-connected and islanded modes. Fig. 2 illustrates the schematic diagram of a three-phase DG system, in which DG interfacing inverter is connected to the PCC with an LCL filter. Local loads are connected at PCC

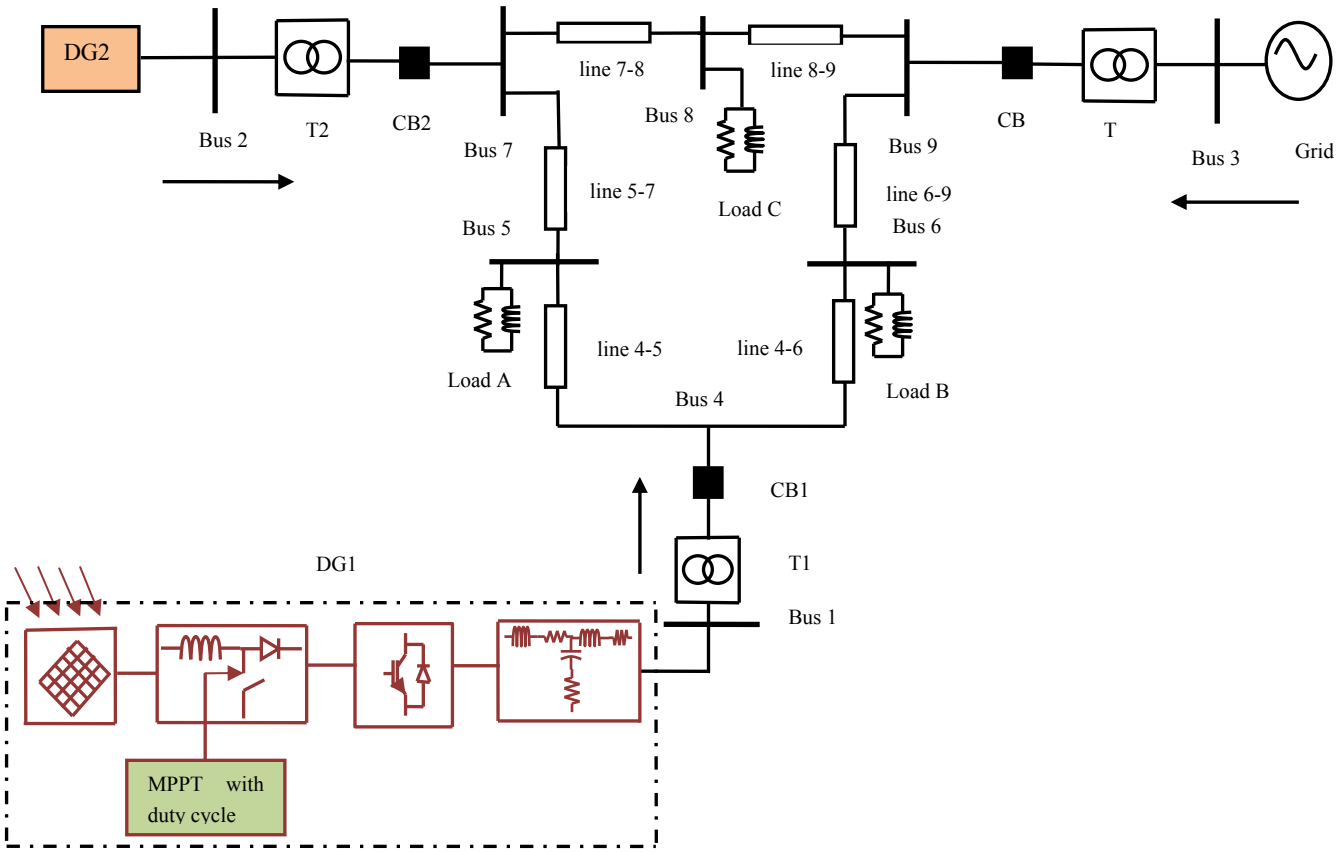

Fig. 1. Single line diagram of the proposed study.

TABLE I
DISTRIBUTION LINE PARAMETERS OF IEEE 9-BUS SYSTEM
(EACH PARAMETER REPRESENTS THE PI SECTION AND RATED KV = 25)

Parameter	R1(Ω)	R0(Ω)	L1(H)	L0(H)	C1(f)	C0(f)	Distance
lines 4–5	0.0529	0.13225	1.192e-3	2.38e-3	8.82e-9	5.188e-9	20km
lines 4–6	0.08993	0.2248255	1.29e-3	3.22e-3	7.922e-9	4.74e-9	20km
lines 5–7	0.16928	0.4232	2.259e-3	5.64e-3	15.34e-9	9.025e-9	100km
lines 6–9	0.20631	0.5157	2.38e-3	6.09e-3	17.95e-9	10.55e-9	100km
lines 7–8	0.044965	0.11241	1.01e-3	2.02e-3	7.471e-9	4.394e-9	100km
lines 8–9	0.062951	0.15737	1.414e-3	3.53e-3	10.47e-9	6.15e-9	100km

TABLE II
BUS PARAMETERS OF IEEE 9 BUS SYSTEM

Bus	Base voltage	Voltage (p.u.)	Phase (degree)
1	425	1.04	0
2	425	1.025	9.173
3	120k	1.025	4.558
4	230k	1.026	−2.226
5	230k	0.9962	−4.002
6	230k	1.032	1.867
7	25k	1.026	3.62
8	25k	1.016	0.632
9	25k	1.032	1.867

and DG locations. The combined control structure is composed of a linear quadratic regulator (LQR) as well as a pre-compensator with an observer for the effective operation of the system as shown in the lower part of Fig. 2. Fig. 3 shows the basic structure of the improved LQR based controller with the addition of the pre-compensator with an observer.

As shown in the upper part of Fig. 2, the DG interfacing inverter and passive filter are considered for the state-space model. The inductor currents and capacitor voltage of the system are chosen as state variables $x = [i_1 \quad i_2 \quad V_c]^T$. The system can be modeled with the state space equation $\dot{x} = Ax + B_1u + B_2u$. On the basis of Fig. 2, the linear differential equations that describe system behavior are expressed as follows.

$$u(t) = R_1 i_1(t) + L_1 \frac{di_1(t)}{dt} + v_c(t) \quad (1)$$

$$i_1(t) = i_2(t) + C \frac{dv_c(t)}{dt} \quad (2)$$

$$v_c(t) = R_2 i_2(t) + L_2 \frac{di_2(t)}{dt} + y(t) \quad (3)$$

Using equations (1) to (3), we describe the state model as follows.

$$A = \begin{bmatrix} -\frac{R_1 + R_f}{L_1} & \frac{R_f}{L_1} & -\frac{1}{L_1} \\ \frac{R_f}{L_2} & -\frac{R_2 + R_f}{L_2} & \frac{1}{L_2} \\ \frac{1}{C} & -\frac{1}{C} & 0 \end{bmatrix} \begin{bmatrix} i_1 \\ i_2 \\ V_c \end{bmatrix},$$

$$B_1 = \begin{bmatrix} \frac{1}{L_1} \\ 0 \\ 0 \end{bmatrix}, \quad B_2 = \begin{bmatrix} 0 \\ -\frac{1}{L_2} \\ 0 \end{bmatrix}, B = [B_1 \quad B_2],$$

$$y = Cx, y = i_2, C = \begin{bmatrix} 1 & 0 & 0 \\ 0 & 1 & 0 \end{bmatrix} \quad (4)$$

An optimal design strategy is then employed to optimize the gain parameters of the system. To obtain the optimal gain, we express the objective function J as follows.

$$J = \frac{1}{2} \sum_{k=0}^{\infty} x^T(k) Q x(k) + u^T(k) R u(k) \quad (5)$$

where Q and R represent the cost of the individual state variables diverging from their operating points and the cost of the control inputs, respectively. By choosing Q and R as positive semidefinite and positive definite matrices, respectively, we obtain $J \geq 0$. The optimal gain matrix K is given by

$$K = R^{-1} B_1^T P \quad (6)$$

where P is a positive definite and symmetric matrix of the order 3 × 3. The solution can be obtained by using the following algebraic Ricati equation:

$$A^T + PA - PB_1^T P + Q = 0 \quad (7)$$

From equations (6) and (7), we can write

$$K = \begin{bmatrix} K_{11} & K_{12} & K_{13} \\ K_{21} & K_{22} & K_{23} \end{bmatrix} \quad (8)$$

The state feedback gain K can be synthesized using the LQR technique. The LQR control law signal is given by

$$u = -K\dot{x} \quad (9)$$

A pre-compensator is employed in the model to reduce steady state errors and settling time. By applying this approach, the operating point of the control system can be adjusted. Let X_{ss} and u_{ss} represent the steady state value with $u(k) = 0$ and the associated control unit, respectively. The main objective of this approach is to adjust the static state feedback control law obtained from equation (9) to achieve the desired steady state value. The approach is performed by using a state vector offset in the control law as follows.

$$u(k) = -K[x(k) - X_{ss}] + u_{ss} \quad (10)$$

$$u(k) = -Kx(k) - KX_{ss} + u_{ss} \quad (11)$$

$$u(k) = -Kx(k) + [K \quad 1] \begin{bmatrix} X_{ss} \\ u_{ss} \end{bmatrix} \quad (12)$$

Using the augmented state vector, we can write

$$\begin{bmatrix} A - I & B \\ C & 0 \end{bmatrix} \begin{bmatrix} X_{ss} \\ u_{ss} \end{bmatrix} = \begin{bmatrix} 0 \\ r \end{bmatrix} \quad (13)$$

Assuming the matrix on the left as non-singular, we can rewrite equation (13) as

$$\begin{bmatrix} X_{ss} \\ u_{ss} \end{bmatrix} = \begin{bmatrix} A - I & B \\ C & 0 \end{bmatrix}^{-1} \begin{bmatrix} 0 \\ r \end{bmatrix} \quad (14)$$

Using equations (11) and (14), we can write the following expressions:

$$u(k) = -Kx(k) + [K \quad 1] \begin{bmatrix} A - I & B \\ C & 0 \end{bmatrix}^{-1} \begin{bmatrix} 0 \\ r \end{bmatrix} \quad (15)$$

$$N = [K \quad 1] \begin{bmatrix} A - I & B \\ C & 0 \end{bmatrix}^{-1} \begin{bmatrix} 0 \\ r \end{bmatrix} \quad (16)$$

This leads to the following control law for pre-compensated static feedback.

$$u(k) = -Kx(k) + Nr \quad (17)$$

Here, N is the feed-forward control gain. Practically, N is obtained from

$$N = -[C(A - BK)^{-1} B + D]^{-1} \quad (18)$$

The closed loop system equations using pre-compensation are as follows:

$$\begin{bmatrix} x(k) = (A - BK)x(k) + BNr(k) \\ y(k) = Cx(k) + DNr(k) \end{bmatrix} \quad (19)$$

To further improve system stability, we introduce an observer with the pre-compensated LQR controller. A full order state observer can be expressed as

$$\hat{x} = (A - LC)x + Bu + Ly \quad (20)$$

where $L = \begin{bmatrix} L_{11} & L_{12} & L_{13} \\ L_{21} & L_{22} & L_{23} \end{bmatrix}$ is the observer gain. The eigenvalues of the observer can be calculated from the characteristic equation $\det(sI - A - LC) = 0$. Three poles $\mu_1, \mu_2,$ and μ_3 of the observer can be a combination of real and complex values. If the Eigenvalues of matrix $(A - LC)$ are selected in such a way that the dynamic behavior of the error vector becomes rapid and asymptotically stable. The observer based controller can be obtained using equations (9) and (20).

$$\hat{x} = (A - LC - BK)x + Ly \quad (21)$$

The transfer function of the observer controller is

$$K(SI - A + LC + BK)^{-1} \quad (22)$$

A stability analysis is performed, and the results for the open loop system, LQR controller, observer controller, and pre-compensator with observer controller are presented in Figs. 4(a)–(d). The dominant poles and zeros of the eigenvalues clearly move to the left of the real axis, thus showing the improved stability of the system. The controller parameters of a single DG system are described in Table III.

IV. Islanding Detection Using Hybrid FRWPT Method

This section briefly describes islanding and its accurate detection with the hybrid FRWPT method. Intentional islanding arises in a microgrid system when the grid side CB is opened because of network faults. In this situation, the microgrid must be operated efficiently by employing the

TABLE III
CONTROLLER PARAMETERS OF SINGLE DG SYSTEM

Parameter	Value	Parameter	Value
Filter resistance ($R_1$and R_2)	0.0019Ω	Filter capacitor	22μF
Filter inductor ($L_1$and L_2)	25mH	DC link voltage	630V
Q	$diag(1 \quad 100 \quad 1)$	R	$\begin{matrix}0.1 & 0\\ 0 & 0.1\end{matrix}$
$K=\begin{bmatrix}K_{11} & K_{12} & K_{13}\\ K_{21} & K_{22} & K_{23}\end{bmatrix}$	$K=\begin{bmatrix}7.1779 & -1.7491 & 1.9636\\ -1.7491 & 3.7198 & 0.7937\end{bmatrix}$	N	$\begin{matrix}-1.3331\\ -38.9220\end{matrix}$
$L=\begin{bmatrix}L_{11} & L_{12} & L_{13}\\ L_{21} & L_{22} & L_{23}\end{bmatrix}$	$L=\begin{bmatrix}-1144 & 1177 & 45467\\ 1210 & 1244 & -45442\end{bmatrix}$	$[\mu_1 \quad \mu_2 \quad \mu_3]$	$[-8 \quad -10 \quad -12]$

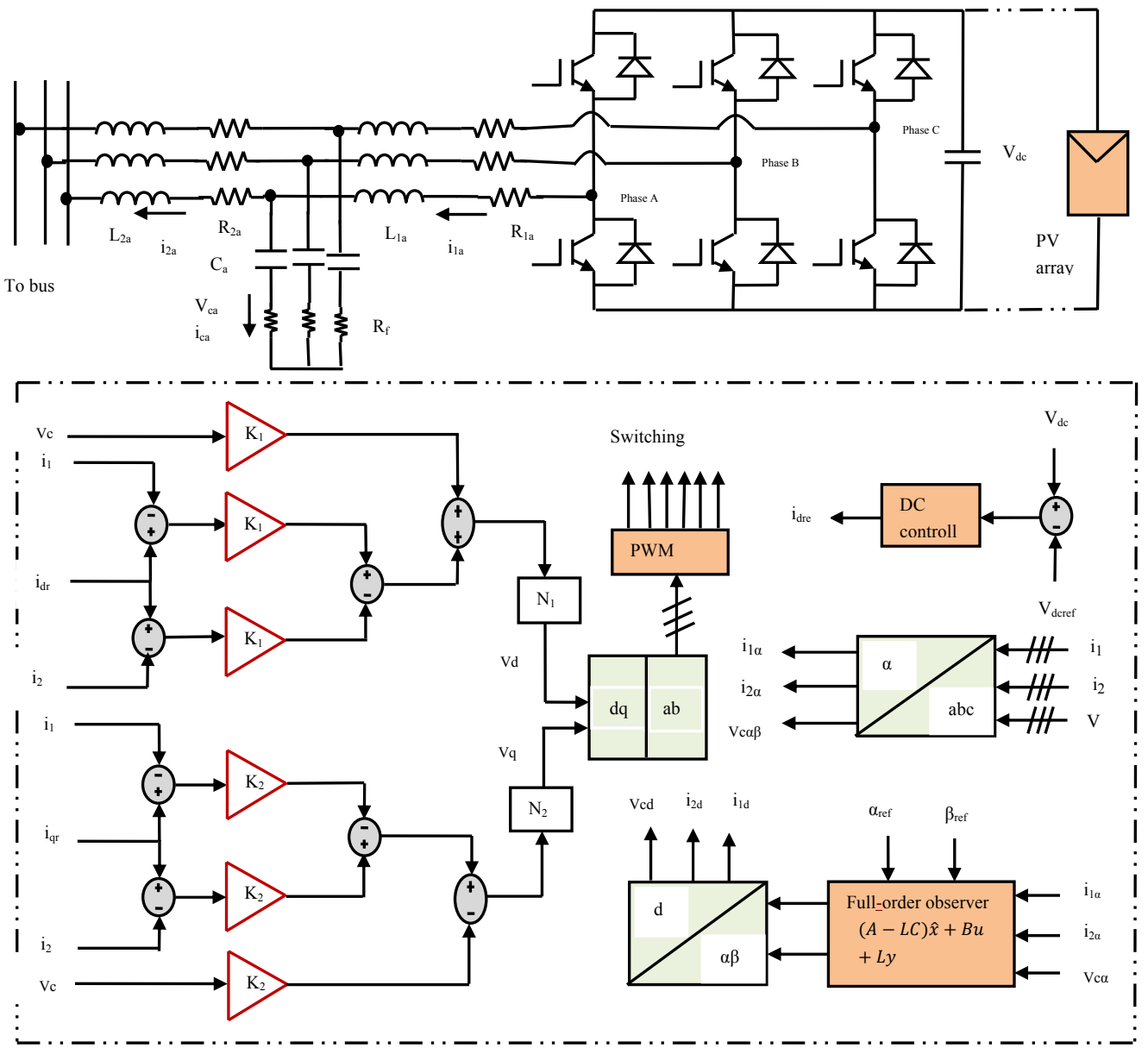

Fig. 2. Schematic diagram of DG system with LQR system based observer controller.

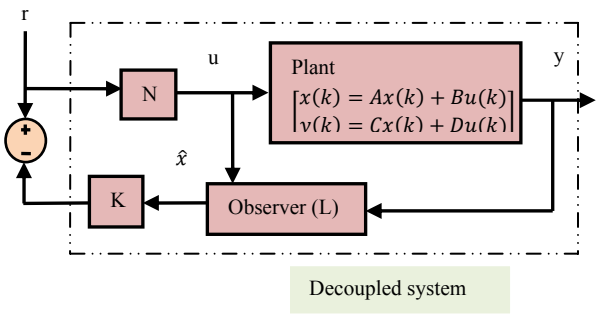

Fig. 3. Controller block diagram of grid-connected system.

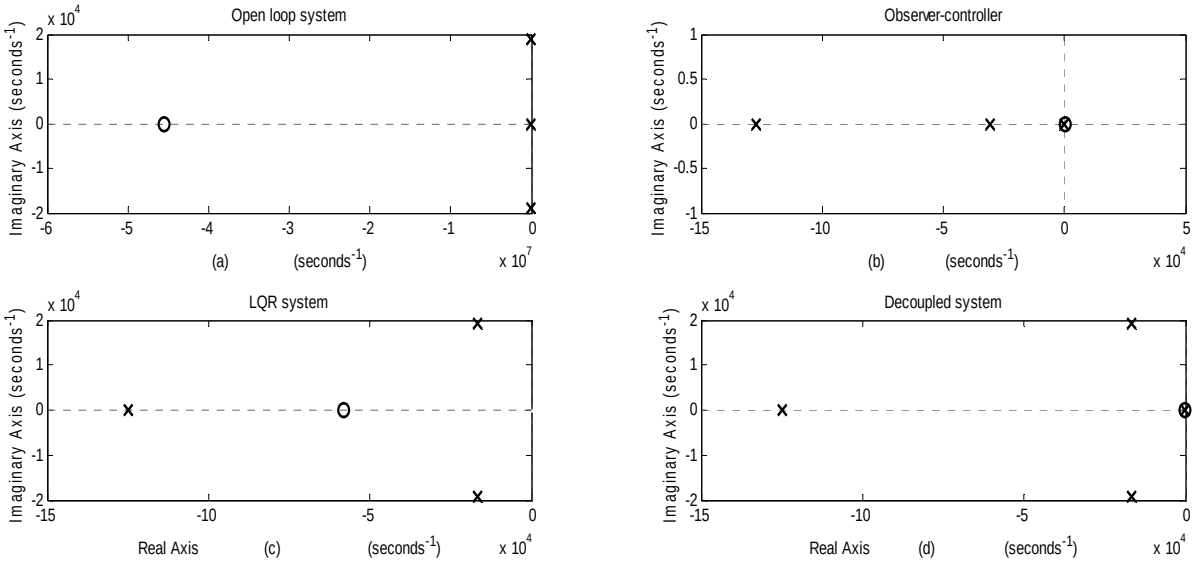

Fig. 4. Pole-zero map for the transfer function of the (a) open loop system, (b) full order observer with LQR controller and (c) with LQR system, and (d) pre-compensator gain with observer controller or decoupled system.

proposed control technique to monitor the power demand by the sensitive loads connected at DG locations. When the microgrid is isolated from the main utility, each DG inverter system must detect the occurrence of islanding to achieve a smooth change in the system operation.

In evaluating the accuracy of islanding detection for grid-connected DG systems in multibus microgrids under various perturbations, a hybrid technique based on the combined desirable features of the WPT and FRFT must be adopted [33]. FRFT exhibits a unitary property in governing the arbitrary angle rotation of the signal to be transformed in the time–frequency plane. Moreover, WPT exhibits a multi resolution property.

Similar to WT, WPT is a highly effective and powerful signal processing technique. It is a generalization of the multi resolution analysis, but its detailed coefficients are also decomposed into equivalent bandwidth data for an accurate analysis. The capability of WPT to analyze non-stationary signals while preserving time and frequency information makes it a suitable islanding detection technique for grid-connected PV systems. The basis functions of WPT are orthogonal time localized signals that offer an inner product between the signals $x[n]$ and the filter coefficients. $g[n]$and $h[n]$ denote the low pass filter (LPF) and high pass filter (HPF) coefficients, respectively. The WPT for the processing of any discrete signal $x[n]$ can be expressed as follows.

$$\Omega[n] = \sum_{k=0}^{N-1} a[n] + \sum_{k=0}^{N-1} d[n] \quad (23)$$

$$d[n] = \sum_{k=0}^{N-1} x[n]h[n-k] \quad (24)$$

$$a[n] = \sum_{k=0}^{N-1} x[n]g[n-k] \quad (25)$$

The digital filter is an important aspect of a wavelet basis function. The memory size, speed, accuracy, and reliability can be optimized by choosing a proper mother wavelet. The minimum description length (MDL) data criteria are used to select a digital filter in the implementation of the WPT technique. Orthogonal wavelet basis functions include the Haar, biorthogonal, symlets, coiflects, Meyer and Daubechies families, etc. However, db4 and db8 of the Daubechies family are mostly used to detect fault signals. In this study, db4 is evaluated by applying an MDL function, which is expressed in equation (26). The MDL function with index k and n is described as follows. Specifically, k and n denote the retained coefficient and the number of wavelet filters, respectively. In

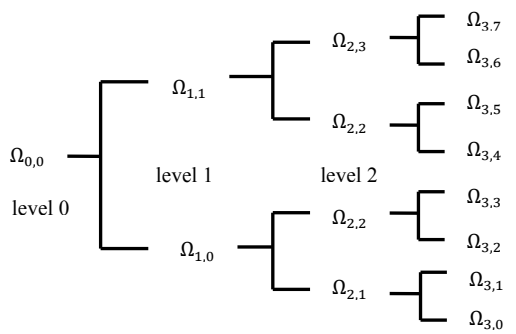

Fig. 5. Two level decomposition of a discrete signal by WPT.

TABLE IV
LPF AND HPF FILTER COEFFICIENTS

$g[n]$	$h[n]$
−0.0105	−0.2303
0.0328	0.7148
0.0308	−0.6308
−0.1870	−0.0279
−0.0279	0.1870
0.6308	0.0308
0.7148	−0.0328
0.2303	−0.0105

addition, N and M denote the length of the signal and the total number of wavelet filters, respectively.

$$MDL(k,n) = \min\{\frac{3}{2}klogN + \frac{N}{2}log\left\|\tilde{\alpha}_{x.j} - \alpha_{x.j}^{(k)}\right\|^2\} \quad (26)$$

$g[n]$ and $h[n]$ are relevant to equation (27) and are regarded as individual coefficients.

$$h_k = (-1)^k g_{L-k}: k = 0,1,2 \ldots L-1 \quad (27)$$

where L represents the finite length of a wavelet space.

$$W_{s,c,b}(n) = 2^{\frac{j}{2}} W_c(2^{-j}(n-b) \quad (28)$$

$$x[n] = \sum_s \sum_c \sum_b W_{s,c,b}[n] W_c[n] \quad (29)$$

where $W_c(n)$ is the WT coefficient matrix. The wavelet packet basis functions $W_{s.c.b}(n)$ are obtained from a single base function or the mother wavelet at scale "s", oscillation "c", and location "b" as described in (28).

Fig. 5 shows the two level decomposition of a discrete signal by applying a WPT based technique with a tree structure. The root of the tree is the original discrete data set. The next step is obtained by applying WPT. The subsequent levels in the tree are constituted by applying WPT on the LPF and HPF, as obtained in the previous step. The coefficients of the LPF and HPF are presented in Table IV.

The output signal $x(n)$obtained by applying the detailed coefficients followed by down sampling is fed to the FRFT based arbitrary angle rotation to achieve an accurate identification even under minute perturbations in the system. By applying FRFT, a signal can be decomposed in terms of chirps. The FRFT is evaluated by employing any arbitrary angle of rotation in the time–frequency plane as the fractional power of the conventional Fourier transform. The advantages of this technique include a single/dual frequency operator, frequency dominance, and successive applications of the FRWPT order. Considering an arbitrary signal $x(u)$, its α^{th} order can be expressed as

$$X_\alpha(u) = \mathcal{F}^\alpha[x(u)] = \int_{-\infty}^{\infty} K_\alpha(u,t)\, x(t) dt \quad (30)$$

where the kernel$K_\alpha(u,t)$is

$$K_\alpha(u,t) = \sqrt{\frac{1-jcot\theta}{2\pi}} e^{j/2(u^2+t^2)\,cot\,\theta - jut\,csc\theta}, \propto \neq k$$
$$\delta(t-u), \propto = 2k$$
$$\delta(t+u), \propto = 2k+1 \quad (31)$$

α can be varied from 0 to1. Then, the resultant WPT signal changes from an input transformation function to Fourier transformation.

The fractional wave packet transform for a given signal $x(t)$ can be defined as

$$(\mathcal{F}^\alpha x)(u,a,b) = \frac{1}{\sqrt{a}} \int_{-\infty}^{\infty} K_\alpha \psi(\frac{\mathrm{t-b}}{\mathrm{a}}) x(t) dt \quad (32)$$

For angles that are not multiples of π, FRWPT can be expressed as

$$(\mathcal{F}^\alpha x)(u,a,b) =$$
$$\sqrt{\frac{1-j\cot\alpha}{2\pi}} e^{j\frac{u^2}{2}\cot\alpha} \int_{-\infty}^{\infty} \psi(\frac{\mathrm{t-b}}{\mathrm{a}}) \mathrm{x(t)} e^{j\frac{t^2}{2}\cot\alpha} e^{jut\ \csc\propto} dt \quad (33)$$

where$K_\alpha$is the kernel of the FRFT.

The FRWPT based islanding detection technique for multi bus microgrid systems can be implemented using the following steps.

Step 1. Initialize the sample index $J = 0$.

Step 2. Extract the active and reactive power from the PCC at every instant.

Step 3. Initialize the samples of S as expressed in (34) under any perturbation. Place the samples in the circular buffer.

$$S = \sqrt{P^2 + Q^2} \quad (34)$$

Step 4. Initialize h[n] using the db4 wavelet in Table IV.

Step 5. Perform a convolution of S with h[n] with down sampling to obtain the detailed coefficients using (24).

Step 6. Initialize αorder optimization.

Step 7. Apply α-order FRFT to the resultant detailed signal using (31).

Step 8. Evaluate $(\mathcal{F}^\alpha x)$ using (33), and check the threshold condition.

Step 9. If the threshold condition is satisfied, execute the trip signal (1→0).

Else: $J = J + 1$, and proceed to **Step 2**.

By applying this proposed combined technique, transform orders play the key role of the algorithm. As described in the subsequent section, the microgrid system is simulated for the accurate and rapid identification of islanding and power quality events.

V. SIMULATION RESULTS AND DISCUSSION

We perform our analysis using MATLAB to validate the use of the proposed hybrid FRWPT detection technique along

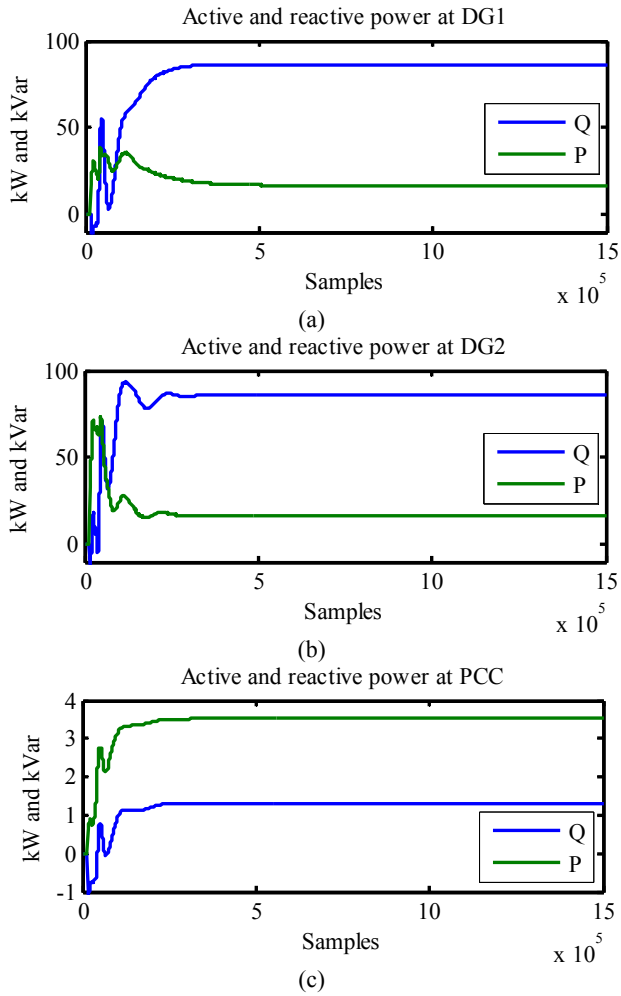

Fig. 6. Power output characteristic for grid-connected mode (a). Power output of DG1. (b) Power output of DG2. (c) Power output of utility grid

with the decoupled controller for microgrid systems under various perturbations. Several test cases are illustrated to examine the steady state and transient behavior of the system operation. A typical microgrid system as shown in Fig. 1 is modeled using SIMULINK built-in blocks. Islanding is detected with zero NDZ, which results from the load demand and inverter output power being exactly equal. The power signals obtained at the PCC are processed through the islanding detection block. In this section, simulation and comparative performance analysis under various islanding and non islanding events are carried out using the WT, WPT, and FRWPT based techniques.

A. Grid-Connected Mode

The objective of this case study is to examine the performance of inverter based DG units and utility grid in delivering power to the local loads connected at DG locations.

Figs. 6(a), (b), and (c) show the power fed by DG1, DG2, and the utility grid, respectively. In this test case, the utility grid behaves as a slack bus that mainly supports real/reactive

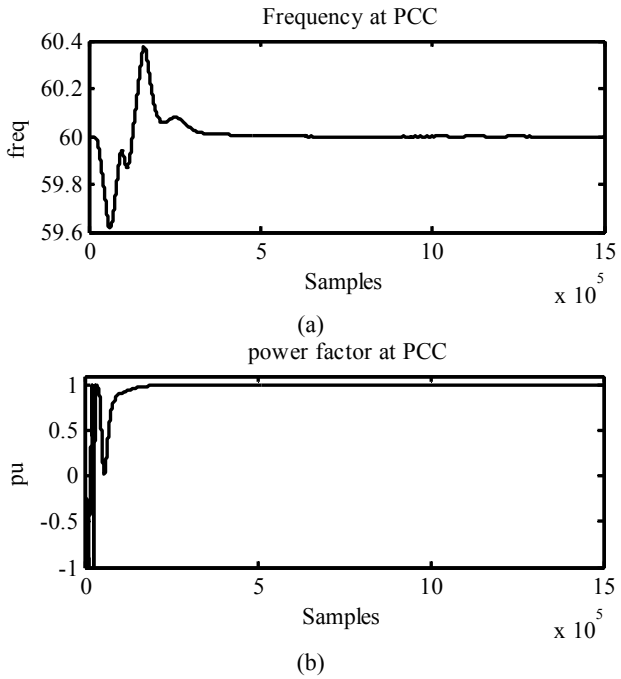

Fig. 7. Frequency and power factor characteristics at PCC under normal condition. (a) Frequency at PCC. (b) Power factor at PCC.

power requirements during any fault condition or load fluctuations. As shown in these figures, the power delivered by DG1, DG2, and the utility grid are 80KW/20KVar, 80KW/20KVar, and 3.5 kW/1.22 kVAR, respectively.

Figs. 7(a) and (b) depict the behavior of the frequency and power factor at the PCC, respectively. Under a steady state, the frequency and power factor reach their respective nominal values.

B. Islanding Mode

Islanding arises by tripping the main CB, as shown in Fig.1. In this case study, we must investigate the transient performance of the microgrid under intentional islanding, including the time of occurrence of such phenomenon. Fig. 8 shows the steady state and transient characteristics of the power fed by the utility grid. Before the occurrence of islanding, the power output of the utility grid is 3.5 kW/1.22 kVAR, which suddenly increases during islanding. As depicted in Fig. 8, a sudden change in power occurs at 5.9e5 samples, and power transient persists until the 9.2e5 samples because of islanding. Under this perturbation, the islanding detection based on the WT, WPT, and FRWPT is depicted from the top to the bottom sections of Figs. 9(a), (b), and (c), respectively. The WPT based detection technique can barely identify the commencement of the disturbance, whereas the WT and FRWPT based detection techniques identify both the commencement and termination of the disturbance. Moreover, the duration of the disturbance in the system can be detected easily and effectively with use of the FRWPT based detection technique.

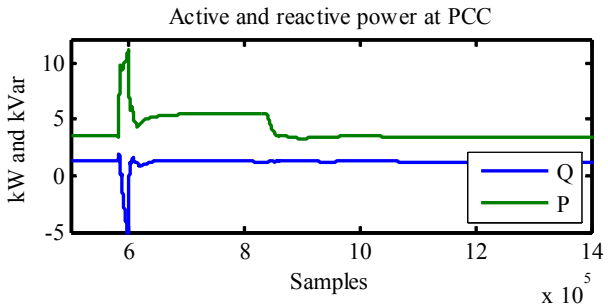

Fig. 8. Power output characteristic at PCC.

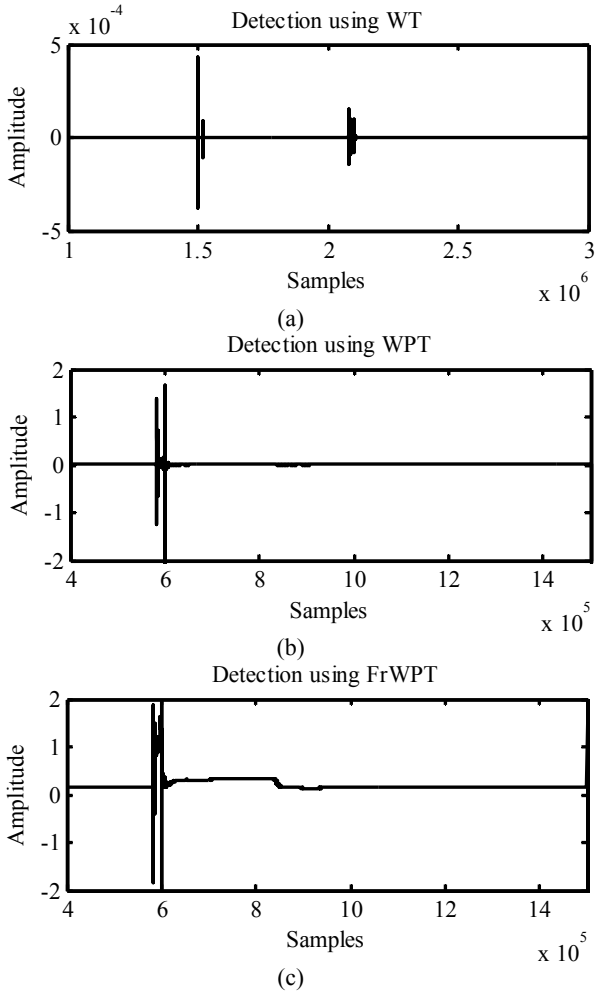

Fig. 9. Islanding detection based on the WT, WPT, and FRWPT techniques.

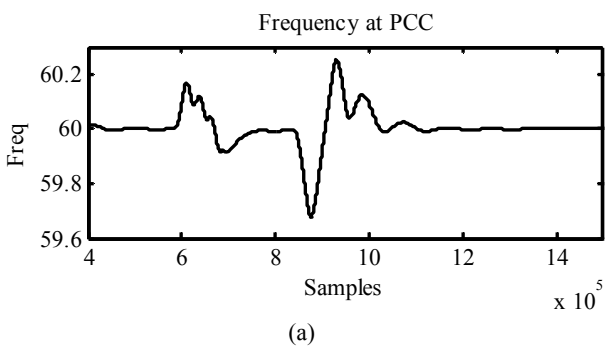

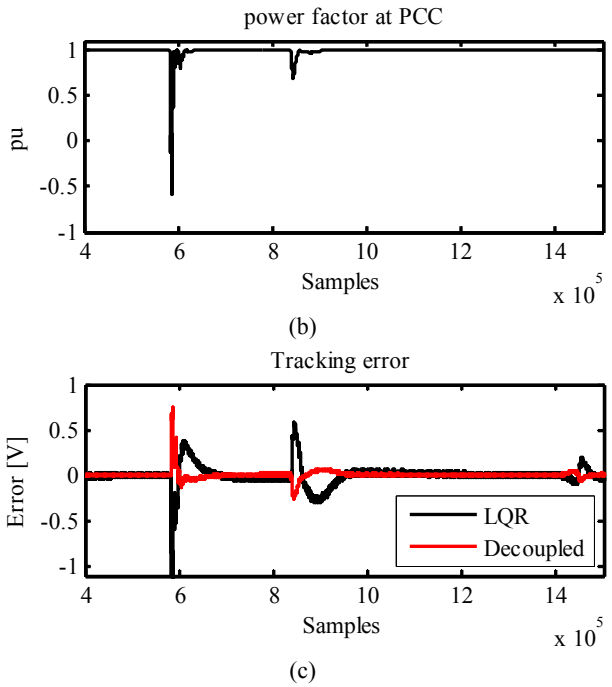

Fig. 10. (a) Frequency at PCC. (b) Power factor at PCC. (c) Tracking error characteristics.

Figs. 10(a), (b), and (c) depict the behavior of the frequency, power factor, and tracking error at the PCC, respectively. Under a steady state, the frequency and power factor reach their respective nominal values. However, the frequency undergoes significant distortion during islanding. As shown in Fig. 10, the tracking error under islanding is decreased with the proposed control technique.

C. DG1 Under Islanding

CB1 as shown in Fig. 1is tripped to isolate DG1 from the microgrid system. In this case study, we investigate the transient performance of the utility grid and the time of isolation. Fig. 11 shows the power output fed by the utility grid. Before the isolation of DG1, the power output of the utility grid is 3.5kW/1.22 kVAR. During the isolation, a small transient increase in power output occurs. Evidently, such condition occurs at 0.75e5 samples and persists until 1.1e6 samples. The islanding detection based on the WT, WPT, and FRWPT under this perturbation is described in Figs. 12(a), (b), and (c), respectively. As shown in these figures, the WT based technique identifies the disturbance at 1.5e6, whereas the WPT and FRWPT based techniques detect not only the disturbance at its commencement and termination but also its duration. Moreover, the persistence of the disturbance in the system can be detected clearly and significantly with the aid of the FRWPT based detection technique.

Figs. 13(a), (b), and (c) show the behavior of the frequency, power factor, and tracking error at the PCC, respectively. Before the isolation of DG1, the frequency and power factor

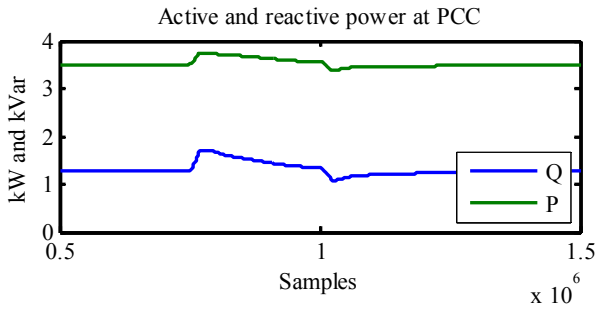

Fig. 11. Power output characteristic at PCC.

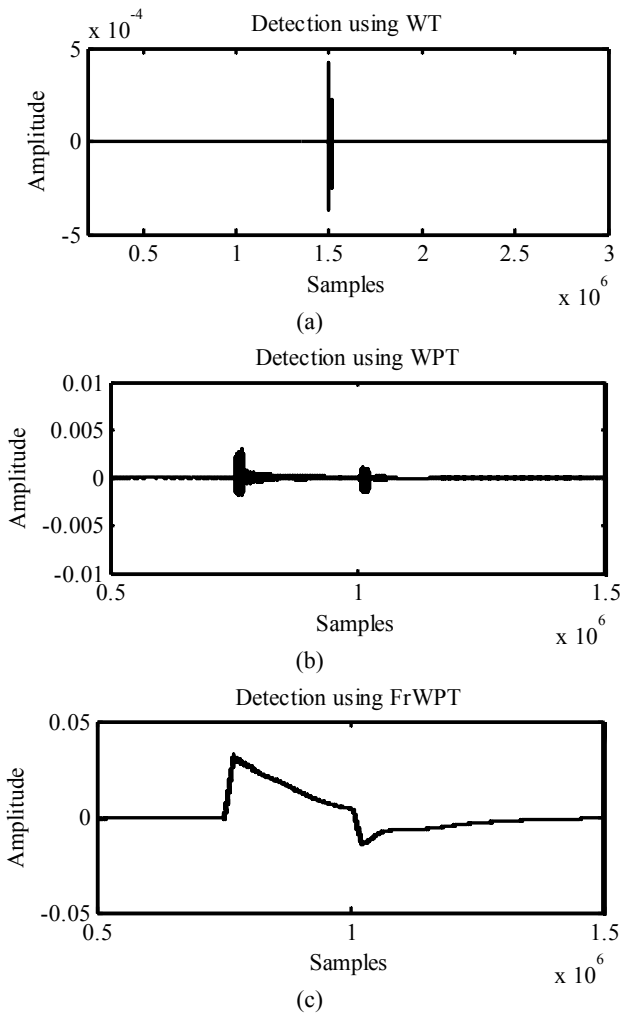

Fig. 12. Islanding detection based on the WT, WPT, and FRWPT techniques.

reach their respective nominal values. However, both the frequency and power factor undergo significant distortion during this DG1 isolation. Under such isolation, the tracking error almost reaches the steady state value throughout the disturbance period via the decoupled control. The LQR based controller exhibits fluctuation around the steady state value.

D. Line-to-Ground (L-G) Fault

A line-to-ground (L-G) fault is created at 1e6 samples, and such fault lasts until 1.28e6 samples, as depicted by the

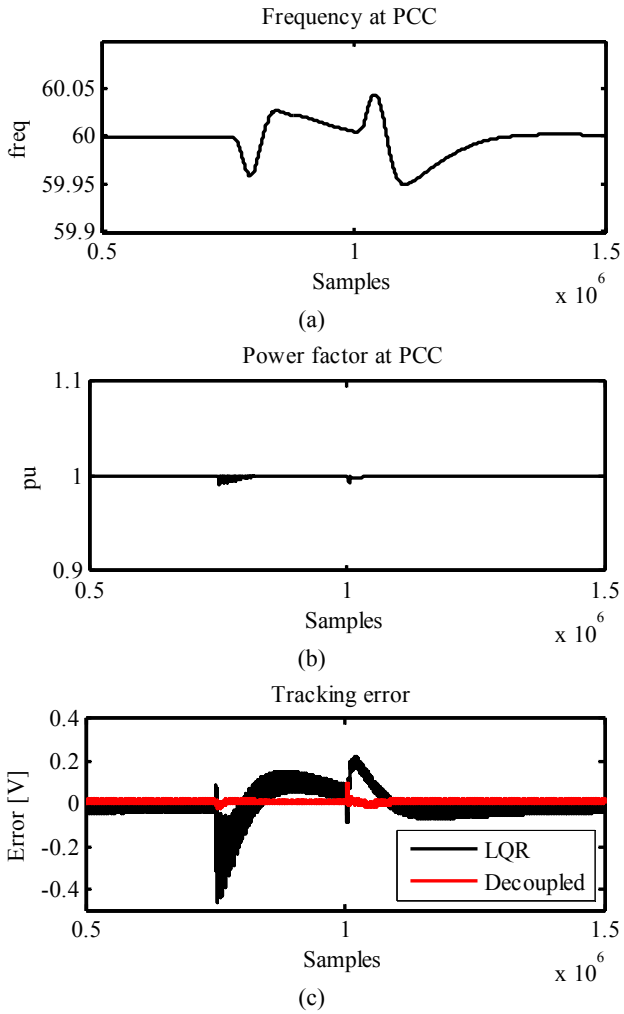

Figs. 13. Frequency, power factor, and tracking error characteristics.

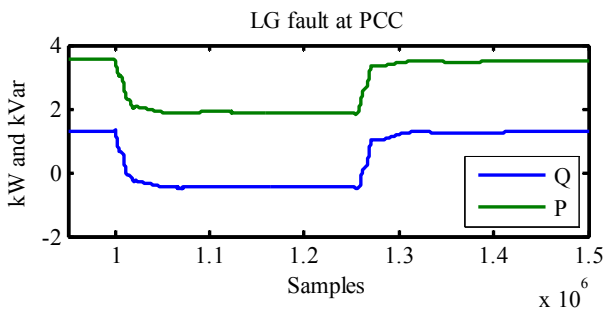

Fig. 14. Power output characteristic at PCC.

power curves in Fig. 14.

The islanding detection based on the WT, WPT, and FRWPT under this perturbation is shown in Fig. 15. The WT based disturbance detection technique achieves detection at 1.5e6 samples, whereas the WPT and FRWPT based techniques achieve accurate detection at the commencement and termination of the disturbance. However, the WPT based detection technique fails to show the duration of such fault occurrence except start and end point.

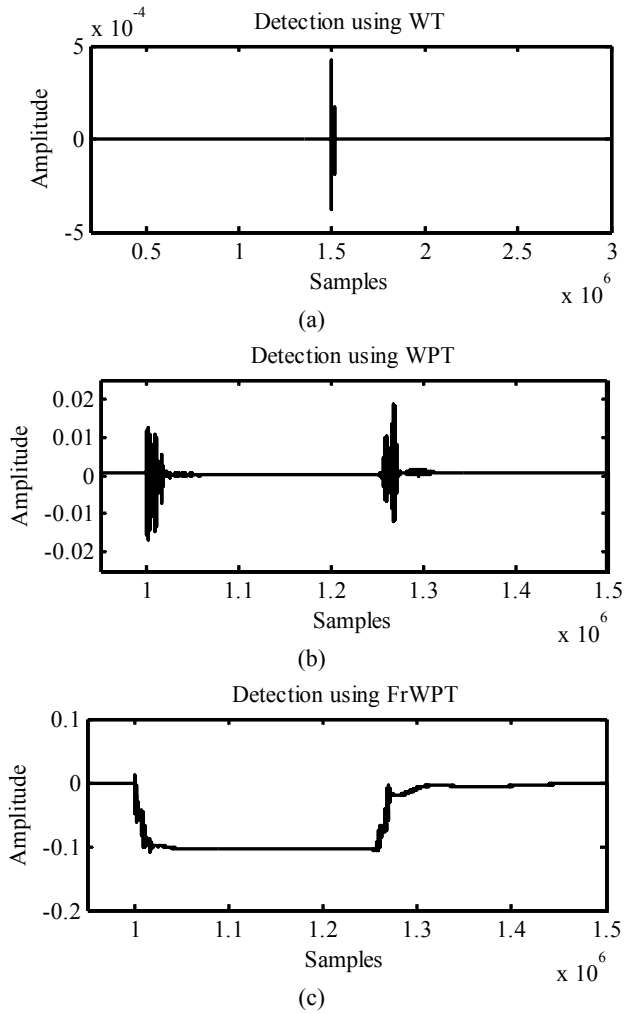

Fig. 15. Islanding detection based on the WT, WPT, and FRWPT techniques.

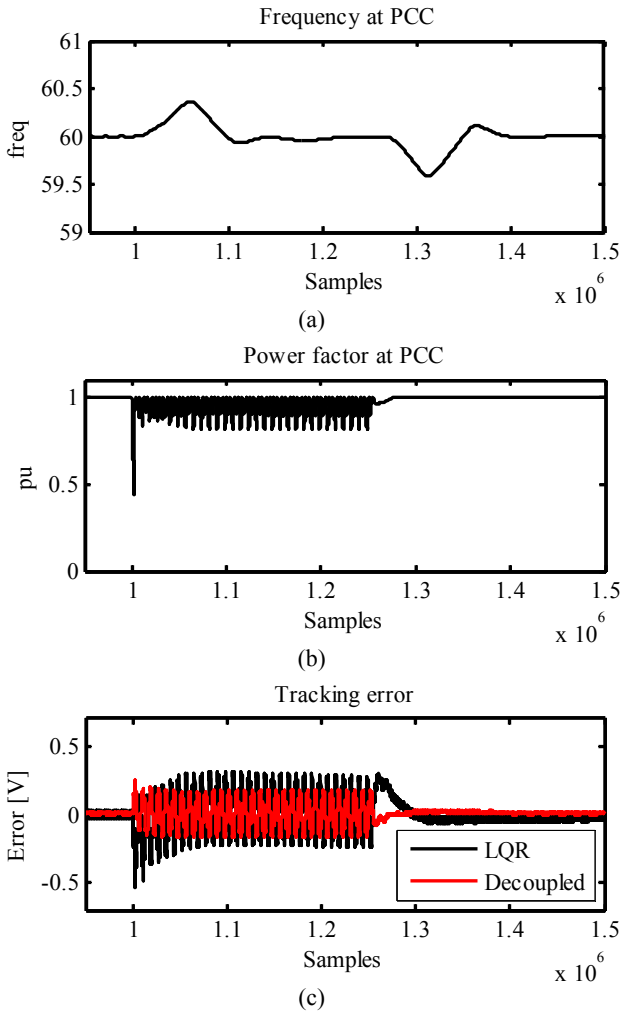

Fig. 16. Frequency, power factor, and tracking error characteristics.

Figs. 16(a), (b), and (c) depict the behavior of the frequency, power factor, and tracking error at the PCC, respectively. The frequency and power factor undergo significant distortion during the occurrence of the L-G fault. However, the tracking error characteristic shows a reduction in the steady state value and settling time with the application of the proposed controller.

E. Line-to-Line (L-L) Fault

A line-to-line (L-L) fault is created at 0.75e6 samples, and such fault lasts until 0.9e6 samples, as represented by the power curves in Fig. 17.

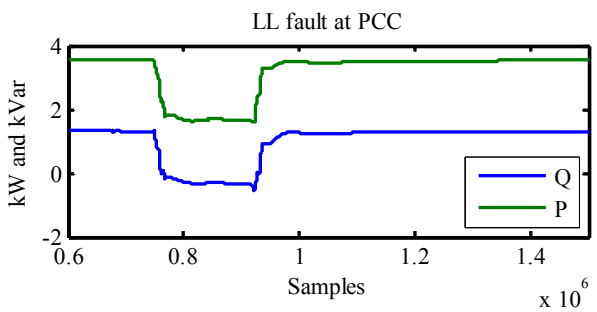

Fig. 17. Power output characteristic at PCC.

Fig. 18 shows that the WT based technique can identify the disturbance at 1.5e6, whereas the WPT and FRWPT based techniques achieve disturbance detection at exactly 0.75e6. Moreover, the duration of the disturbance in the system can be detected easily and significantly with the FRWPT based detection technique.

Figs. 19(a) and (b) show that the frequency and power factor undergo significant distortion during this L-L fault. The tracking error under this event, as shown in Fig. 19(c), is

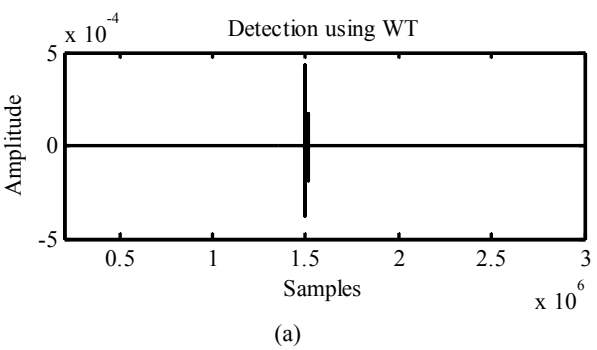

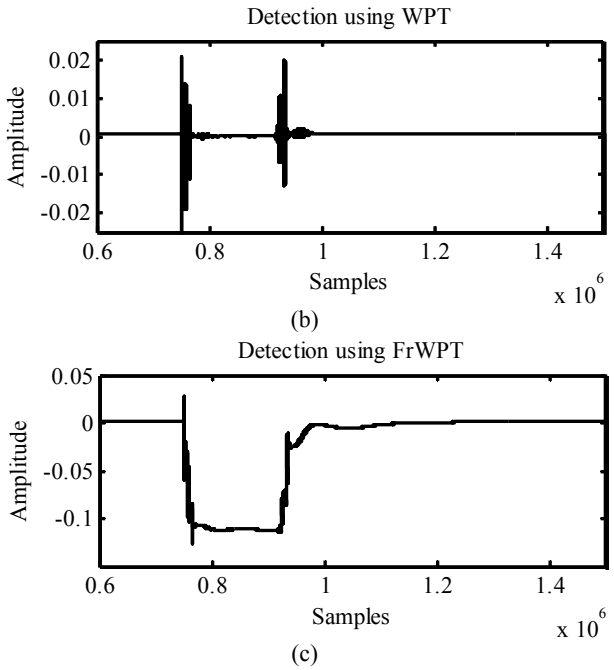

Fig. 18. Islanding detection based on the WT, WPT, and FRWPT techniques.

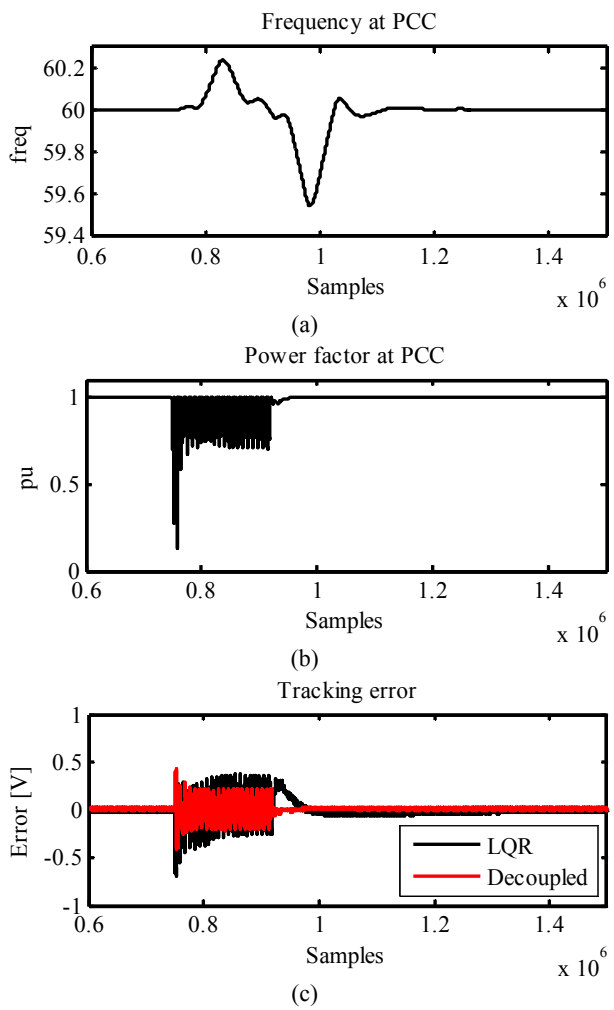

Fig. 19. Frequency, power factor, and tracking error characteristics.

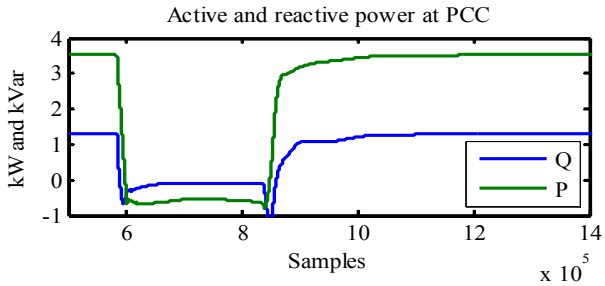

Fig. 20. Power output characteristic at PCC.

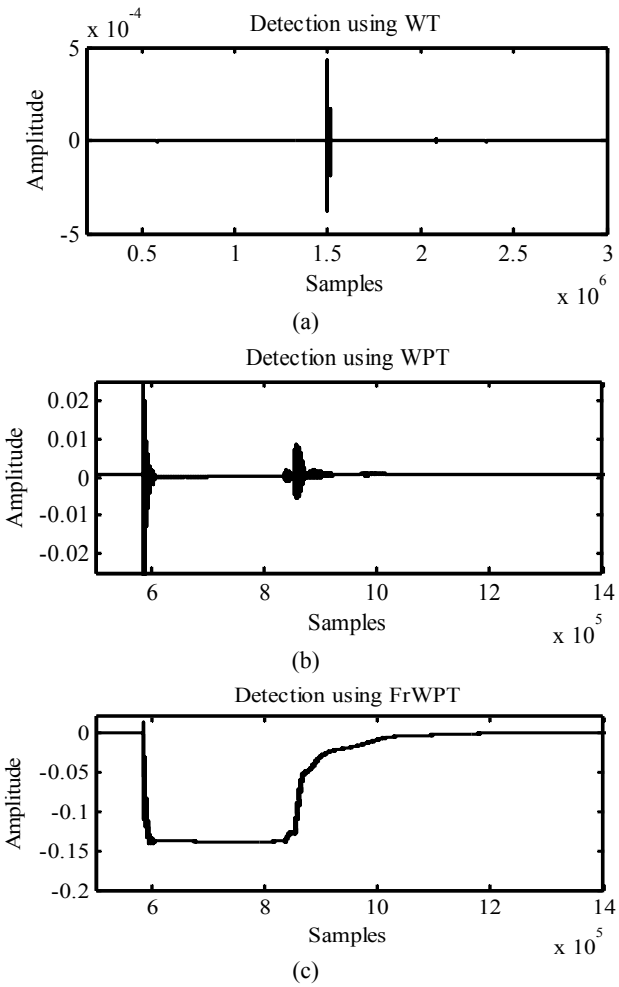

Fig. 21. Islanding detection based on the WT, WPT, and FRWPT techniques.

decreased up to a steady state value within a short period using the decoupled technique.

F. Dynamic Load Change

In this case, the load at bus 6 is changed from linear to nonlinear, as depicted in Fig. 20. This nonlinear load persists from 5.8e6 to 8.5e6. Fig. 21 shows that detection under this change is accurate and visualized throughout.

Fig. 22 shows the frequency, power factor, and tracking error under this scenario. Both the frequency and power factor are disturbed. Moreover, the tracking error based on

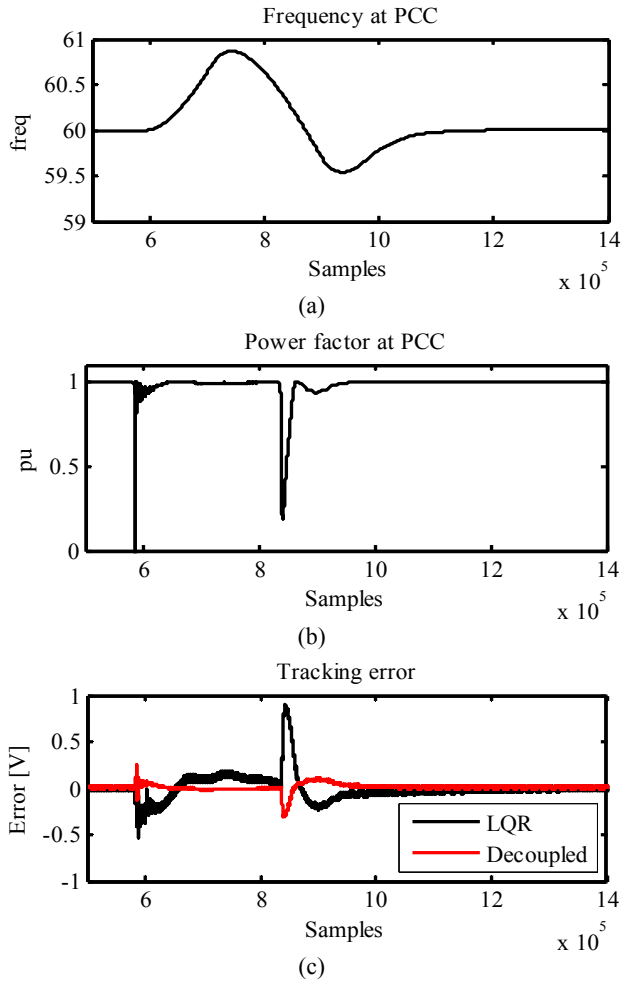

Fig. 22. Frequency, power factor, and tracking error characteristics.

the proposed controller is superior to that based on the conventional controller.

G. Voltage Dip

Voltage dip arises because of the drop from 120kV to 80kV at bus 3 of the microgrid system during 6.8e5 to 9.5e5 samples as shown in Fig. 23. Under this scenario, the detection is performed and compared by applying the WT, WPT, and FRWPT based techniques. These characteristics are depicted in Fig. 24, which indicates that the fault detection performed with the FRWPT technique is relatively accurate and prominent. Fig. 25 shows the characteristics of the frequency, power factor, and tracking error. Evidently, the power factor remains constant at unity. However, the frequency undergoes distortion at the commencement and termination of the disturbance. Moreover, unlike that based on the conventional LQR controller, the tracking error based on the proposed controller is almost zero, except for a small change at the transient points.

A comparative performance analysis of the different detection techniques employed to identify various power

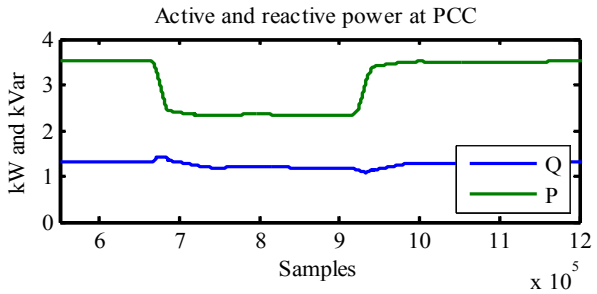

Fig. 23. Power output characteristic at PCC.

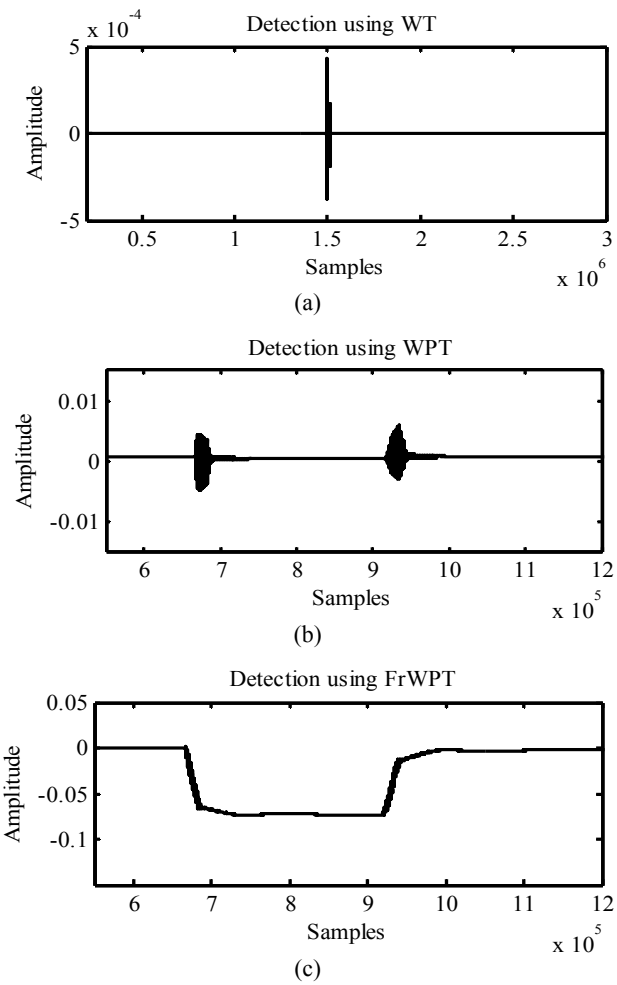

Fig. 24. Islanding detection based on the WT, WPT, and FRWPT techniques.

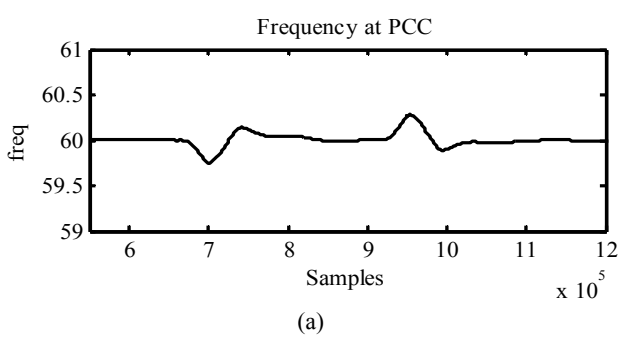

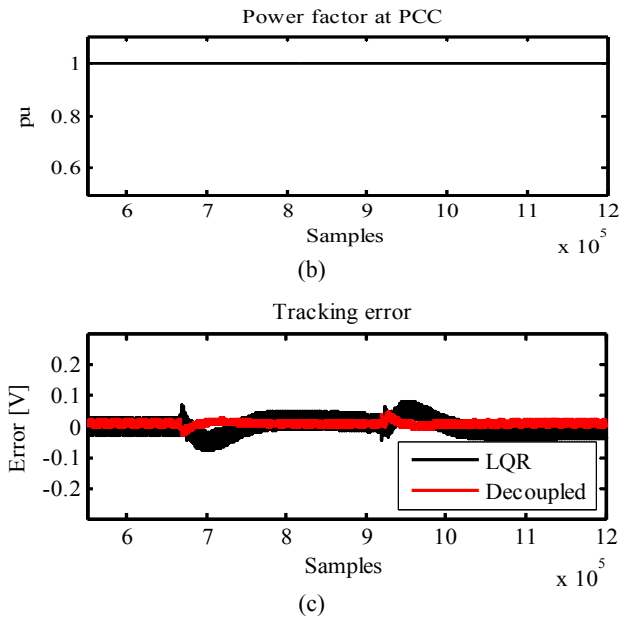

Fig. 25. Frequency, power factor, and tracking error characteristics.

TABLE V
COMPARATIVE ANALYSIS OF DIFFERENT DETECTION TECHNIQUES

Islanding/non-islanding events	Beginning and end of events (in samples)	WT	WPT	FRWPT
Utility is OFF	t_{ds}=5.9e5	1.5e6	5.9e5	5.9e5
	t_{de}=9.2e5	2.2e6	UI	9.2e5
DG1 isolated	t_{ds}=0.75e6	UI	0.75e6	0.75e6
	t_{de}=1.1e6	1.5e6	1.05e6	1.1e6
L-G fault	t_{ds}=1e6	UI	1e6	1e6
	t_{de}=1.28e6	1.5e6	1.27e6	1.28e6
L-L fault	t_{ds}=0.75e6	UI	0.75e6	0.75e6
	t_{de}=0.9e6	1.5e6	0.8e6	0.92e6
Load change	t_{ds}=5.8e6	UI	5.9e6	5.8e6
	t_{de}=8.5e6	1.5e6	8.3e6	8.5e6
Voltage dip	t_{ds}=6.8e5	UI	6.9e5	6.8e5
	t_{de}=9.5e5	1.5e6	9.4e5	9.6e5

t_{ds}*=event starting time; t_{de}*=event ending time; UI*=Unidentified

quality events is described in Table 5. The FRWPT based technique accurately identifies the commencement, termination, and duration of the events.

VI. CONCLUSIONS

A hybrid FRWPT detection technique, as well as a decoupled controller, is employed to achieve efficient operation, protection, and islanding detection for a multibus microgrid system. The improved decoupled control technique is applied in this study to monitor the real and reactive powers of DG units under grid-connected and islanded modes. The simulated results show that the tracking error under various power quality disturbances reaches a steady state value with negligible oscillation with the use of the proposed control technique. Furthermore, this work presents a comparative performance analysis of islanding and non-islanding detection using the FRWPT, WPT, and WT algorithms. As mentioned previously, WT based detection is not accurate. By contrast, the FRWPT based technique accurately identifies different transient disturbances of the microgrid system, including their commencement and termination. The proposed FRWPT based detection technique achieves the desired objectives in a rapid, accurate, and robust manner that justifies its effectiveness.

REFERENCES

[1] J. M. Carrasco, L. G. Franquelo, J. T. Bialasiewicz, E. Galvan, R. C. Portillo Guiesado, M. A. M. Prats, J. I. Leon, and N. Moreno-Alfonso, "Power electronic systems for the grid integration of renewable energy sources: A survey," *IEEE Trans. Ind. Electron.*, Vol. 53, No. 4, pp. 1002-1016, Jun. 2006.

[2] M. Hamzeh, H. Karimi, and H. Mokhtari, "Harmonic and negative-sequence current control in an islanded multi-bus MV microgrid," *IEEE Trans. Smart Grid*, Vol. 5, No. 1, pp. 167-176, Jan. 2014.

[3] F. Gao and M. R. Iravani, "A control strategy for a distribuited generation unit in grid-connected and autonomous modes of operation," *IEEE Trans. Power Del.*, Vol. 23, No. 2, pp. 850-859, Apr. 2008.

[4] F. Blaabjerg, R. Tedorescu, M. Liserre and A. V. Timbus, "Overview of control and grid synchronization for distributed power generation systems," *IEEE Trans. Ind. Electron.*, Vol. 53, No. 5, pp. 1398-1409, Oct. 2006.

[5] M. Liserre, F. Blaabjerg, and S. Hansen, "Design and control of an LCL filter based three-phase active rectifier," *IEEE Trans. Ind. Appl.*, Vol. 41, No. 5, pp. 1281-1291, Sep./Oct. 2005.

[6] Y. Li, D. M. Vilathgamuwa, and P. C. Loh, "Design, analysis and real-time testing of a controller for multibus microgrid system," *IEEE Trans. Power Electron.*, Vol. 19, No. 5, pp. 1195-1204, Sep. 2004.

[7] M. Bouheraoua, J. Wang, and K. Atallah, "Design and implementation of an observer-based state feedback controller for a pseudo direct drive," *IET Electr. Power Appl.*, Vol. 7, No. 8, pp. 643-653, Sep. 2013.

[8] B. Li, M. Zhang, L. Huang, and L. M. Tolbert, "A new optimized pole placement strategy of grid-connected inverter with LCL-filter based on state variable feedback and state observer," *IEEE Conference*, pp.2900-2906, 2013.

[9] S. E. Saarakkala and M. Hinkkanen, "State-space speed control of two-mass mechanical systems: Analytical tuning and experimental evaluation," *IEEE Trans. Ind. Appl.*, Vol. 50, No. 5, pp. 3428-3437, Sep./Oct. 2014.

[10] M. A. Mahmud, M. J. Hossain, H. R. Pota, and A. M. T. Oo, "Robust nonlinear distributed controller design for active and reactive power sharing in islanded microgrids," *IEEE Trans. Energy Convers.*, Vol. 29, No. 4, pp. 893-903, Dec. 2014.

[11] K. N. E. K. Ahmad, J. Selvaraj, and N. A. Rahim, "A review of the islanding detection methods in grid connected PV inverters," *Renewable and sustainable Energy Reviews*, Vol. 21, pp.756-766, May 2013.

[12] F. De Mango, M. Liserre, A. Dell'Aquila, and A. Pigazo, "Overview of anti-islanding algoithms, Part-I: Passive methods," *12th International power electronics and motion control conference (EPE-PEMC)*, pp. 1878-1883, 2006.

[13] F. De Mango, M. Liserre, A. Dell'Aquila, and A. Pigazo, "Overview of anti-islanding algoithms, Part-I: Active methods," *12th International power electronics and motion control conference (EPE-PEMC)*, pp.1884-1889, 2006.

[14] C. L. Tryillo, D. Velasco, E. Figueres, and G. Garcera, "Analysis of active islanding detection methods for grid connected micro inverters for renewable energy processing," *Applied Energy*, Vol. 87, No. 11, pp. 3591-3605, Nov. 2010.

[15] P. Mahat, Z. Chen, and B. Bak-Jensen, "A hybrid islanding detection technique using average rate of voltage change and real power shift," *IEEE Trans. Power Del.*, Vol. 24, No. 2, pp. 764-771, Apr. 2009.

[16] J. A. Laghari, H. Mokhilis, M. Karimi, A. H. A. Bakar, and H. Mohamad, "Computational intelligence based techniques for islanding detection of distributed generation in distribution network: A review," *Energy conversion and Management*, Vol. 88, pp. 139-152, Dec. 2014.

[17] S. R. Mohanty, N. Kishor, P. K. Ray, and J. P. S. Catalão, "Comparative study of advanced signal processing techniques for islanding detection in a hybrid distributed generation system," *IEEE Trans. Sustain. Energy*, Vol. 6, No. 1, pp.122-131, Jan. 2015.

[18] S. J. Pinto and G. Panda, "Wavelet technique based islanding detection and improved repetitive current control for reliable operation of grid-connected PV systems," *Journal of Electrical Power and Energy Systems*, Vol. 67, pp. 39-51, May 2015.

[19] P. K. Ray, S. R. Mohanty, and N. Kishor, "Disturbance detection in grid-connected distributed generation system using wavelet and S-transform," *Electr. Power Syst. Res*. Vol. 81, No. 3, pp. 805-819, Mar. 2011.

[20] Z. L. Gaing, "Wavelet based neural network for power disturbance recognition and classification," *IEEE. Trans. Power Del*., Vol. 19, No. 4, pp. 1560-1568, Oct. 2004.

[21] M. A. S. K. Khan, T. S. Radwan, and M. A. Rahman, "Wavelet packet transform protection of disturbances in three-phase interior permanent magnet motor fed from sinusoidal PWM voltage source inverter," *IEEE Conference on CCECE.CCGEI*, pp. 178-181, 2006.

[22] S. J. Pinto and G. Panda, "Performance evaluation of WPT based detection for grid-connected PV systems," *Journal of Electrical Power and Energy Systems*, Vol. 78, pp. 537-546, Jun. 2016.

[23] S. A. Saleh, A. S. Aljankawey, R. Meng, J. Meng, C. P. Diduch, and L. Chang, "Anti islanding protection based on signatures extracted from the instantaneous apparent power," *IEEE Trans. Power Electron.*, Vol. 29, No. 11, pp. 5872-5891, Nov. 2014.

Smitha Joyce Pinto was born in Mangalore, Karnataka, India. She received her B.E. degree in Electronics and Communication from SJCE, VTU University, Mysore, India, and her M.E. degree in Biomedical Instrumentation from the Cummins College of Engineering for Women, Pune University, India, in 2004 and 2012, respectively. She is working toward her Ph.D. degree in the Department of Electrical Engineering at NIT Meghalaya, India. She has five years of teaching experience in the field of electronics engineering. Her research interests are control and islanding in distributed generation, microgrids, and biomedical instrumentation.

Gayadhar Panda was born in Odisha, India, in 1970. He received his bachelor's degree from the Institute of Engineers, India, in 1996. He obtained his post graduation from Bengal Engineering College, India, and his Ph.D. degree from Utkal University, India, in 1998 and 2007, respectively. He has 17 years of teaching experience in the field of electrical engineering. Since January 2013, he has been with the Department of Electrical Engineering, National Institute of Technology Meghalaya, India, where is currently an Associate Professor. His research interests include automatic generation control, stability improvements using FACT devices, power quality, power electronic converters, and renewable energy.